J Appl Electrochem (2011) 41:1175–1182
DOI 10.1007/s10800-011-0335-7

ORIGINAL PAPER

Polarization curve analysis of all-vanadium redox flow batteries

Doug Aaron · Zhijiang Tang · Alexander B. Papandrew · Thomas A. Zawodzinski

Received: 20 May 2011 / Accepted: 8 July 2011 / Published online: 18 August 2011

Abstract We outline the analysis of performance of redox flow batteries (RFBs) using polarization curves. This method allows the researcher immediate access to sources of performance losses in flow batteries operating at steady state. We provide guidance on 'best practices' for use of this tool, illustrated using examples from single cells operating as vanadium redox batteries.

Keywords Flow battery · Polarization curve · Vanadium redox battery · VRB · RFB

1 Introduction

Redox flow batteries (RFBs) have drawn considerable interest from energy storage researchers for a variety of reasons [1–3]. In contrast with batteries such as lead-acid, Ni–Cd and Li-ion that store charge in the solid state, charge in RFBs is typically stored in solution. Anolyte and catholyte solutions containing reversible redox couples are stored separately, and passed through a flow cell for charge and discharge. This effectively decouples the power density and energy capacity of RFBs, resulting in flexibility in battery system design. Currently, RFBs are widely considered a promising energy storage candidate for coupling with intermittent power sources, such as wind and photovoltaic cells, and for loading leveling for the electrical grid [4–6].

A commonly investigated RFB chemistry is the all-vanadium system, for which sulfuric acid solutions of the V^{2+}/V^{3+} and V^{4+}/V^{5+} (present as VO^{2+}/VO_2^{+}) redox couples serve as the anolyte and catholyte, respectively. During battery discharge, VO_2^{+} is reduced to VO^{2+} at the cathode, accompanied by a concomitant oxidation of V^{2+} to V^{3+} on the anode; these reactions proceed in the opposite direction in the charging process.

Typical testing of modifications to RFBs involves charge–discharge cycling to determine the voltage, charge, and power efficiency. However, cycling experiments do not provide direct information on which mechanisms result in RFB efficiency loss. Polarization curves are commonly used in fuel cell studies to analyze the losses in a cell. Polarization curves with associated cell resistance measurements provide a clear interpretive tool for identifying dominant limitations in performance. The primary losses identified in fuel cells via analysis of polarization curves include kinetic activation polarization, ohmic polarization due to DC resistance and catalyst layer mass transport losses, and mass transport limitation arising from gas transport through gas diffusion media [10]. Kinetic activation polarization is a result of slow charge transfer reactions at the interface between the electrode and electrolyte and is evident at low cell operating current density. Ohmic loss in the cell includes the resistance to ionic transport through the electrolyte (electrolyte solution and the separator-typically a polymer membrane), electrical resistance in the electrodes, and contact resistance between cell components. Finally, concentration polarization dominates when mass transport of reactants limits the current density of a cell [11]. It should be noted that these polarization losses in a cell are not discrete or exclusive, but that

D. Aaron · Z. Tang · A. B. Papandrew · T. A. Zawodzinski (✉)
Department of Chemical and Biomolecular Engineering, University of Tennessee, Knoxville, TN 37996, USA
e-mail: tzawodzi@utk.edu

T. A. Zawodzinski
Physical Chemistry of Materials Group, Oak Ridge National Laboratory, Oak Ridge, TN 37831, USA

all of them contribute to loss in a cell whenever current is flowing. However, each mechanism tends to dominate in different regions of a polarization curve [12].

Flow batteries are similar to fuel cells in important respects. Steady-state performance can be achieved in RFBs given the constant supply of reagent during operation at a stoichiometric flow rate above that demanded by the current density. Nonetheless, polarization curves are underutilized in RFB studies. In this contribution, we explore the application of this simple yet powerful tool to unraveling the performance limitations of vanadium redox cells. We illustrate the method and provide some guidance on its use to extract maximum information from experimental studies.

2 Method

2.1 Cell construction

Two single-cell versions of VRB configurations were utilized in this work. The first was a simple battery (SB) with symmetric carbon felt electrodes housed in PVC compartments. Square PVC pipe formed the electrode compartments, and PVC plates were used as endplates. Viton gaskets were placed between all parts of the cell to ensure no leakage of electrolyte. Polypropylene compression fittings (1/8″ NPT × ¼″ OD tube) were used to connect the electrolyte feed lines to the electrode compartments. A 20 cm^2 Nafion 117 membrane (Ion Power) was used as the separator. Two pieces of graphitic carbon felt (CeraMaterials, 1.27 cm thick, 0.12 Ω cm uncompressed through-plane resistivity) were stacked in each electrode resulting in a total, uncompressed electrode thickness of 2.54 cm. However, because the PVC electrode compartment was intentionally made slightly undersized, the carbon felt electrodes were compressed by approximately 25%. Platinum wires (Alfa Aesar) were inserted into the carbon felts through septa in the endplates to serve as current collectors.

The second cell used in this work was a modified direct methanol fuel cell (DMFC) from Fuel Cell Technologies with an active area of 5 cm^2, hereafter referred to as the 'fuel cell battery' (FCB). The FCB uses Poco graphite plates with single-serpentine flow fields (0.787 mm wide and 1.02 mm deep) for electrolyte delivery and gold-plated aluminum current collectors. Toray carbon paper (0.200 mm thickness, 0.08 Ω cm through-plane resistivity) or carbon felt (initially ~2.5 mm thick, compressed to ~0.500 mm thick, 0.15 Ω cm uncompressed, through-plane resistivity) served as electrodes. We denote the FCB sub-configurations with carbon paper or carbon felt electrodes FCB-P and FCB-F, respectively. In both cases, Nafion®117 was used as the membrane material.

Figure 1 includes schematics of the FCB (Fig. 1a) and the SB (Fig. 1b) indicating the relative sizes of the electrodes and membranes.

2.2 Electrolyte system

An all-vanadium electrolyte was used in this work. 99.9% $VOSO_4$ (Alfa Aesar) was dissolved in 2.0 or 5.0 M H_2SO_4, at a concentration of 0.5 or 1.0 M, respectively. Both sides of the VRB were initially loaded with the V^{4+} solution. The first charging step converted V^{4+} to V^{3+} and V^{5+} in the negative and positive electrode compartment respectively. The V^{5+} solution was removed and replaced with an equal amount of V^{4+} solution, and the VRB was charged again to reach the "fully charged" state consisting of V^{2+} on the anode side and V^{5+} on the positive side. Diaphragm metering pumps (STEPDOS 08 from KNF Lab) delivered electrolyte to the batteries at a flow rate ranging up to 30 mL/min. A nitrogen purge was fed to the negative electrode reservoir (containing V^{2+} and V^{3+}) to avoid

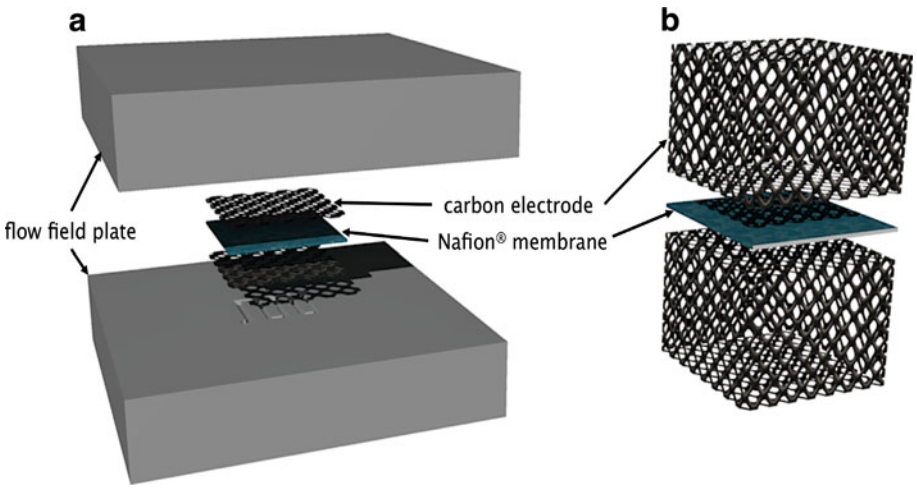

Fig. 1 Schematics of the **a** FCB and **b** SB with carbon felt electrodes

oxidation of the V^{2+} when the battery was in a charged state.

2.3 Electrochemical measurements

In this work, the cells were controlled via a Bio-Logic HCP-803 high current potentiostat/galvanostat/EIS. This potentiostat had a maximum current of 400 mA on the main board and was capable of reaching 80 A via an integrated booster. The working electrode lead from the potentiostat was connected to the positive electrode (V^{4+}/V^{5+}) of the battery while the counter electrode lead was connected to the VRB negative electrode. Polarization curves were generally measured using controlled current steps, measuring the cell potential at each steady-state current value. Cases employing potentiostatic control are noted where appropriate. For a discharging polarization curve measurement, we generally started with a fully charged battery. Charging polarization curves were performed on either fully discharged or partially charged cells. A steady current below 2 mA/cm^2 at a cell potential of 1.8 V was taken to indicate "full charge." The cell was charged or discharged at the specified current for 30 s and then allowed to rest for up to 2 min at its open circuit voltage (OCV). Following this open circuit period, the next desired current in the polarization curve was set by the potentiostat. Cell potential measurements were averaged over the 30 s of each current step to provide a point on the polarization curve. The electrolyte flow rate for these measurements ranged from 10 up to 30 mL/min. All experiments were carried out at room temperature (25 °C), with no active control exerted on the temperature of the cell or the electrolyte solutions. However, the temperature change between inlet and outlet at maximum power was measured to be ~1 °C. Thus, we can safely assume approximately constant temperature conditions.

Prior to and following each polarization curve, the high frequency resistance (HFR) was measured for the VRB. The potentiostat measured the HFR at 15–30 kHz using an AC potential perturbation of 10 mV amplitude, measuring the current response. This resistance was multiplied by the active area of the membrane (5 or 20 cm^2, depending on the battery type) to determine the areal specific resistance (ASR) of the cell and to iR correct the cell potential measurements using current density. All reported current densities are with respect to the geometric surface area of the electrode.

3 Results and discussion

Our primary goal in this contribution is the illustration of the use of polarization curves, with cell resistance measurements, in the determination of sources of performance loss in RFBs. This entails an explication of these sources of loss. In general, voltage drops in the cell are associated with (1) electrode polarization or kinetic losses, (2) iR losses, associated with contact and ionic resistances, or 'pseudo-iR' losses, associated with mass transfer of redox-active species within active electrode layers and (3) mass transfer-limiting currents associated with bulk reagent delivery to the electrode. These are listed in order of increasing overvoltage at which they become relevant and are illustrated in Fig. 2. We note that the two sources of loss listed in item (2) could each result in a linear decrease in voltage with increasing current density in the middle portion of the polarization curve. They are, however, readily distinguished by correction of the polarization curve voltage by iR_{dc} where R_{dc} refers to the DC resistance or HFR of the cell. The mass transfer losses within the electrode do not contribute to this HFR resistance since the electrode is electronically shorted in any DC or HFR measurement. We note in passing that the condition of linear voltage drop from catalyst layer loss strictly occurs only when one transport mechanism dominates the voltage drop. However, this linear behavior is often seen in iR-corrected fuel cell polarization curves. Item (3) can be driven by mass transport within flow fields or within an electrode structure and is generally associated with electrode 'starvation', i.e. complete conversion of all available electroactive species at the demanded current density. For analysis of RFBs, care must be taken to ensure that the flow rate of the electroactive electrolyte is substantially in excess of any limiting currents (see below).

3.1 Polarization curves for discharge

Our initial experiments focused on the SB. The electrolyte was 0.5 M $VOSO_4$ in 2.0 M H_2SO_4 fed at a flow rate of

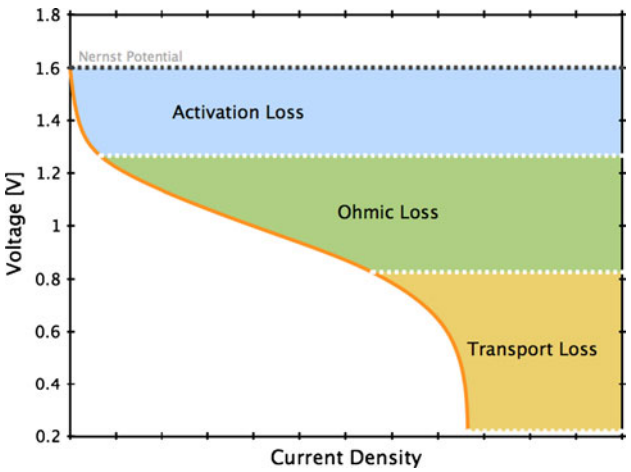

Fig. 2 Generalized polarization curve for a VRB indicating the dominant source of overpotential in each region

30 mL/min. Figure 3 shows the polarization curve results for this experiment. This cell exhibited very little kinetic polarization (~0.031 V drop at 10 mA/cm^2), but a substantial ohmic ASR (4.57 Ω cm^2) and a mass-transport limited current density of 152 mA/cm^2. For comparison, well-hydrated fuel cell configurations using N117 exhibit an ASR of roughly 0.2 Ω cm^2. Clearly, there is a substantial excess resistance in the SB—roughly 200-fold above that of a simple hydrated membrane. We note that a Nafion membrane exposed to this electrolyte composition exhibits comparatively slight changes in conductivity [13]. Nevertheless, the large iR correction applied to the curve removes nearly all polarization, resulting in a flat corrected curve. The predominantly ohmic nature of the voltage loss, given the limited ionic contribution from the membrane, suggests that contact resistance is the primary loss channel in this device. We also largely discount a substantial contribution to ohmic drop arising from the electronic resistance of the carbon electrode material. Even for an uncompressed electrode, the loss associated with this source amounts to only <0.4 Ω cm^2 given the resistivity of material mentioned above. Upon compression, the thickness is decreased as is the resistivity. It is also unsurprising that using a simple wire as a current collector can contribute such a large contact resistance. The impact of this choice of current collector on current distribution in the cell is unclear, but the in-plane resistivity is likely to be substantially lower than that measured through plane. Thus, the lateral iR drop across the electrode is likely somewhat lower than that through the electrode. Further study of this point is beyond the scope of this paper, especially since we regard this geometry to be an extreme and not a viable approach to high-performance cells, in spite of its prevalence in the literature.

Again, the overall points of the above discussion are not only the cell design but also the relative ease of

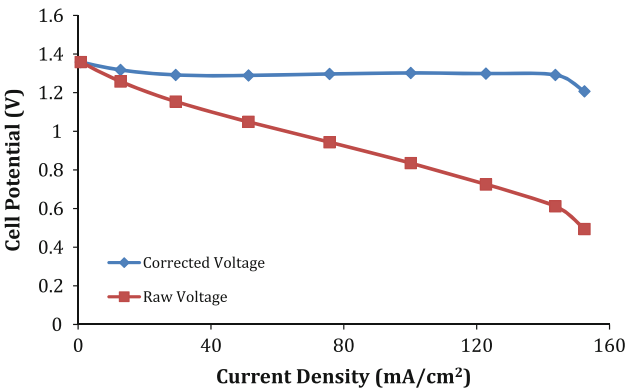

Fig. 3 Discharging polarization curve of the SB illustrating the significant effect iR correction can have on the shape of the curve. Here, the measured ohmic ASR was 4.57 Ω cm^2. The 0.5 M V/2.0 M H_2SO_4 electrolyte flow rate was 30 mL/min

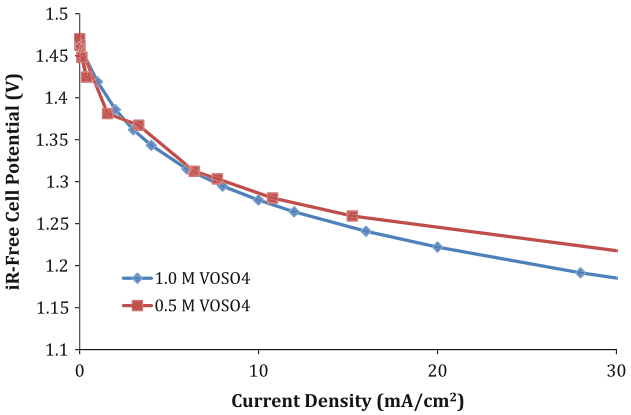

Fig. 4 The effects of electrolyte concentration on the iR-free kinetic region of polarization curves for the FCB-F. The electrolyte solvent in both cases was 5.0 M H_2SO_4

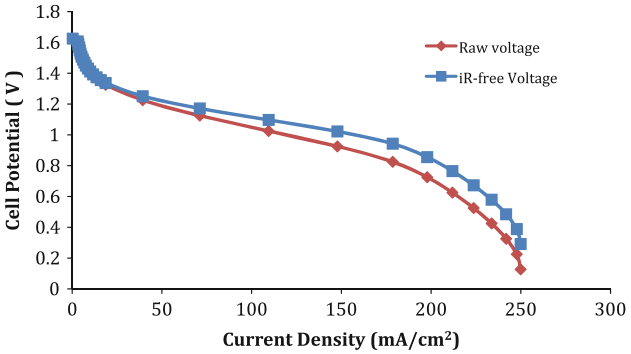

Fig. 5 Discharging polarization curve for the FCB-P showing the magnitude of the iR correction given an ohmic ASR of 0.66 Ω cm^2. The 1.0 M V/5.0 M H_2SO_4 electrolyte flow rate was 12 mL/min

interpretation of the data when obtained as a polarization curve coupled with an HFR/ASR measurement. This analysis reveals, virtually at a glance, the conclusion that losses due to electrode kinetics and mass transport issues are minimal compared to iR losses.

In experiments with both configurations of the FCB, a higher concentration of electrolyte was used. For comparison purposes, the FCB-F was operated with 1.0 M $VOSO_4$ in 5 M H_2SO_4 to examine whether electrolyte concentration had a significant effect on the kinetic region of the polarization curve. Figure 4 illustrates that the kinetic region of the polarization curve, up to ~15 mA/cm^2, was largely unaffected by the increased concentration. Thus, we consider differences in behavior between the SB and FCB to be more due to cell architecture than to any concentration effect.

Figure 5 shows a polarization curve for the FCB-P with a N117 membrane fed with the higher concentration electrolyte (1.0 M $VOSO_4$ in 5 M H_2SO_4) at 12 mL/min. The electrodes in this study were the 0.200 mm thick Toray carbon papers. In this case, kinetic polarization is quite

pronounced compared to the polarization curve for the SB—a drop of 0.215 V at 10 mA/cm^2 in the FCB-P compared to 0.031 V at 10.0 mA/cm^2 in the SB. In contrast with the SB, the ohmic ASR of the FCB-P was 0.660 Ω cm^2. Moreover, the effect of iR correction on the polarization curve was quite different for the FCB-P compared to the SB. In the case of the FCB-P, significant voltage loss is evident after the iR_{dc} correction, indicating that the resistance to charge transport in the mixed conductor is of greater magnitude than ionic or contact resistances. Beyond 180 mA/cm^2, the polarization of the FCB-P becomes mass-transport controlled, reaching a diffusion-limited current density of 250 mA/cm^2. These results suggest that performance in the FCB-P is controlled by a combination of kinetic and active layer mass transport losses.

The FCB-P exhibited much greater kinetic polarization than the SB and iR_{dc} correction did not remove all of the ohmic polarization in the FCB-P. However, the mass transfer limitation generally occurred at higher current density in the FCB-P than it did in the SB. The greater current density associated with mass transfer limitation could be due to improved electrolyte flow across the electrodes and membrane afforded by the graphite flow fields in the FCB-P.

We further investigated the effects of electrolyte transport on polarization in the FCB-P by systematically varying the electrolyte flow rate. These measurements were performed with 1.0 M V/5 M H_2SO_4 electrolyte solutions, a N117 membrane, and carbon paper electrodes. The flow rate was varied from 0.5 up to 25 mL/min. While all other polarization curves in this work had step times of 30 s at a desired current or potential, this series of experiments required step times of 120–180 s to maintain adequate electrolyte circulation at low flow rates and to obtain stable current measurements. The results of these experiments are shown in Fig. 6.

As the flow rate was increased, the onset of mass transport control occurred at progressively lower cell potential and greater current density. Increasing the flow rate from 0.5 to 25 mL/min increased the limiting current density from 40 to 325 mA/cm^2, an eight-fold increase. For comparison, the SB achieved a limiting current density of approximately 165 mA/cm^2 at an electrolyte circulation rate of 30 mL/min.

The high current region of the curves for flow rates of 20 and 25 mL/min displayed an unusual feature: the current density decreased as the cell potential was lowered. This is likely due to depletion of the electrolytes at very high current density. The experiments performed at 20 and 25 mL/min resulted in the state of charge ending below 80% of full charge (76 and 73%, respectively). All of the other polarization curves in this series ended with states of charge

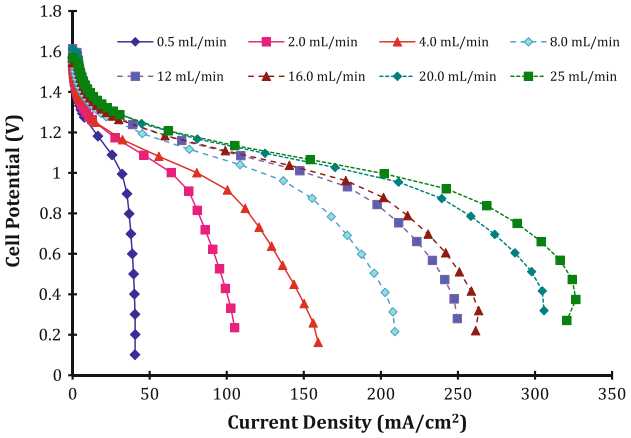

Fig. 6 iR-free discharging polarization curves illustrating the effect of electrolyte flow rate on the FCB-P configuration. The electrolyte consisted of 1.0 M V/5.0 M H_2SO_4

significantly above 80% of full charge (see below). This points to the importance of operating at very low utilization of the overall inventory of the available redox active species over the course of a polarization experiment. In our small laboratory-scale set-up, we are operating with limited electrolyte reservoirs of up to 250 mL volume. While utilization of the available vanadium will lead to a drop in the OCV, the maximum drop in state of charge corresponds to a loss of only ~30 mV. This magnitude of change does not significantly alter any of the conclusions below.

The pronounced effects of electrolyte flow rate on the mass-transport limited current density was surprising and motivated us to calculate the utilization factor for various electrolyte flow rates and to compare these values with the observed limiting current density in the FCB-P.

In Table 1, we present the theoretical limiting current density calculated by converting the delivery rate of electrolyte to the FCB-P to the number of electrons available if all vanadium was converted in a single pass. The observed

Table 1 Comparison of theoretical limiting current density and observed limiting current density in the FCB-P at various electrolyte flow rates

Flow rate (mL/min)	Theoretical limiting current density (mA/cm^2)	Observed limiting current density (mA/cm^2)	Percent of max current
0.5	161	40	25.2
2	643	105	16.3
4	1287	159	12.4
8	2573	209	8.12
12	3860	250	6.48
16	5147	261	5.07
20	6433	306	4.76
25	8042	321	3.99

limiting current density values were taken from the results shown in Fig. 6. At low flow rates, nearly 25% of all the electrons available in the entering vanadium species were harvested in one pass through the FCB-P. However, the limiting current density was quite small—40 mA/cm^2. At the highest flow rate, single-pass utilization of the vanadium was much lower, with only 3.99% of the available electrons transferred to the electrode. This indicates that a greater stoichiometric flow results in improved limiting current density at the cost of utilizing very little of the available vanadium in the electrolyte. Since the vanadium is never really depleted at the electrode surface at high flow rate, mass transfer limitation happens at a much greater current. RFBs are generally recirculating systems, however, making this only negative from the standpoint of increased pump load.

One striking difference evident between the SB and FCB (regardless of FCB electrode material) is the lack of kinetic polarization in the SB. While the carbon felt used in both battery systems was not characterized by a technique such as nitrogen adsorption to determine surface area, the minimal kinetic polarization shown in Fig. 3 is likely to be due to the very large surface area afforded by $\sim$57 cm^3 of carbon felt. For comparison to the 19.1 mm electrode thickness in the SB, the electrodes used in the FCB had thicknesses of approximately 0.50 and 0.20 mm for the carbon felt and carbon paper, respectively. The mass of the carbon felt electrodes in the SB was approximately 3.81 g on each side while the carbon felt electrodes in the FCB-F were approximately 0.10 g each.

It is unlikely that the difference in kinetic region behavior between the SB and FCB originates from the use of different electrolyte concentrations. Though the SB was operated with the less concentrated electrolyte (0.5 M $VOSO_4$ in 2 M H_2SO_4) while the FCB was generally operated with the higher concentration electrolyte (1.0 M $VOSO_4$ in 5 M H_2SO_4). Figure 4 shows that the kinetic polarization in the FCB-F with carbon felt electrodes does not vary with electrolyte concentration. Carbon paper was used for the experiment shown in Fig. 5, and these curves show similar kinetic polarization. Thus, regardless of electrode material and electrolyte concentration, substantial kinetic polarization occurred in the FCB but not in the SB. Carbon paper was not considered as electrode material in the SB since the point of the SB was to have a large, three-dimensional electrode. We surmise that the observed difference is one related to available surface area for the reaction. Detailed studies of electrode kinetics for various materials are underway and will be reported elsewhere.

Another noticeable difference between the polarization curve behavior between the SB and FCB was that iR_{dc} correction removed nearly all of the ohmic polarization present in the SB. We note that the membrane resistance in this system cannot account for the observed ASR. Because the carbon felt electrodes were not compressed to a great degree in the SB (only compressed to 75% of the uncompressed thickness), contact resistance could be very significant in this system, as noted above. Significant contact resistances may exist between the carbon felt electrodes and the N117 membrane and between the active electrodes and current collectors. The current collector was a thin platinum wire that did not share very much contact area with the carbon felt and lacked a robust mechanical connection. If most of the ohmic polarization was primarily due to those two contact resistance mechanisms, such a large effect from iR_{dc} correction is reasonable. On the other hand, the electrodes in the FCB (carbon paper or carbon felt) were under substantial compression against the membrane and the planar flow field plate, and so contact resistances were likely to be very small. In the case of the carbon paper electrodes, the gaskets around the 0.20 mm thick electrodes were 0.15 mm thick, enforcing compression of the carbon paper. Similarly, the 2.5 mm thick carbon felt electrodes had 0.500 mm of gasketing, with an attendant compression resulting. Since both electrodes had substantial pressure on them (the tie-rods were tightened to 11 Nm of torque), contact between the current collectors, electrodes and membrane was expected to be quite good. This is supported by the observation that iR_{dc} correction did not remove all of the ohmic polarization in the FCB. The latter observation is itself an interesting point as it suggests that substantial 'pseudo-iR' loss is present due to mass transport within the active layer of the FCB electrodes. These electrodes are relatively thin (compared to the SB electrode) but are quite thick when compared to a fuel cell electrode. Moreover, these Toray carbon papers are wet-proofed with PTFE for the purpose of water management in PEM fuel cells. In the case of RFBs, such a hydrophobic surface may prevent complete wetting of the electrode by the electrolyte. We thus assign the larger losses in the kinetic region to the smaller available surface area in the FCB electrodes.

3.2 Polarization curves for charging cycles

In addition to discharging polarization curves, charging polarization curves have been considered. Figure 7 includes an example of charging and discharging polarization curves for the FCB-F that have been corrected for iR_{dc}. In this figure, we plotted overpotential versus current density for the convenience of the reader and to make the comparison more transparent. The charging polarization curve was performed with electrolytes at an approximate SOC of 89% following 150 mA discharge for 2 h. The higher concentration electrolyte (1.0 M $VOSO_4$ in 5 M H_2SO_4) was used at a flow rate of 10 mL/min. A N117

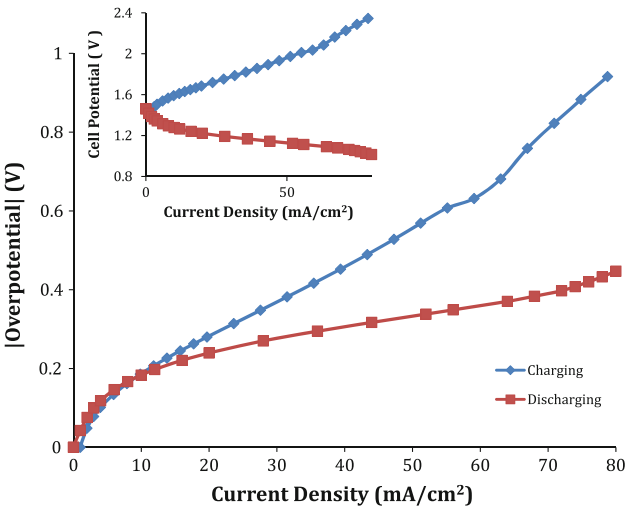

Fig. 7 Absolute value of overpotential for iR-free charging and discharging polarization curves for the FCB-F (the iR-free polarization curves are included in the *inset*). The SOC of the battery was 100% during the discharge curve and 89% during the charge curve. The 1.0 M V/5.0 M H_2SO_4 electrolyte flow rate was 10 mL/min

membrane separated the two carbon felt electrodes. The kinetic polarizations observed were nearly identical, 0.187 V at 10 mA/cm^2 for the charging curve, compared to 0.184 V at 10 mA/cm^2 for the discharging curve. Similarly, the ASR values measured are nearly the same; ASRs of 0.670 and 0.650 Ω cm^2 were measured during charge and discharge, respectively.

Though the curves are very similar at low current density, the charging overpotential deviates from the discharging overpotential at cell operating currents exceeding 15 mA/cm^2. The nearly identical activation overpotentials and ohmic resistances observed during charge/discharge suggest that ionic transport, and not charge transfer, is the source of the observed asymmetry in the data. The onset of mass transfer limitation occurred at similar current densities for charging and discharging, though it did result in a steeper curvature for the charging process than for discharging. Thus, in this case, the primary asymmetry between the discharge and charge curves occurs in the 'pseudo-iR' region of the curve.

In addition to our polarization studies, we also made standard battery cycling measurements. Figure 8 shows the cycling behavior of the FCB-F with a N117 membrane, high concentration electrolyte, and carbon felt electrodes. Cycling was performed at 40 mA/cm^2. Over the course of two cycles, the voltage efficiency of the FCB-F was 79.9 and 78.8%, and the OCV was stable at approximately 1.41 V, indicating little crossover through the membrane or via any cross-membrane leak. These performance metrics are well in line with those reported by other investigators [2, 7–9] and indicate that the FCB is an appropriate model system for the techniques described here.

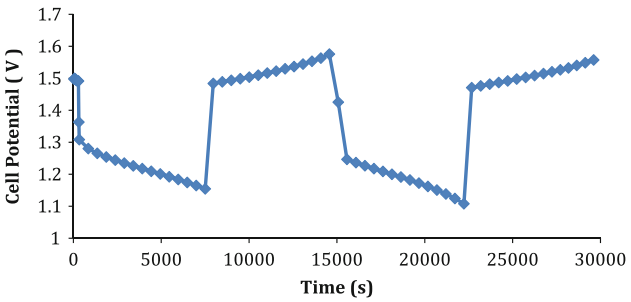

Fig. 8 Cycling behavior of the FCB-F at 40 mA/cm^2 and 30 mL/min 1.0 M V/5.0 M H_2SO_4 electrolyte flow rate. The voltage efficiency of the first cycle was 79.9%

Table 2 Comparison of overpotential, ASR and limiting current for various VRBs

Battery	η_{Cell} at 10 mA/cm^2 (mV)	ASR (Ω cm^2)	$J_{Limiting}$ (mA/cm^2)
SB	31	4.57	160
FCB-F	184	0.65	178
FCB-P (25 mL/min flow)	215	0.63	326
Ref. [15]	~100	5.4	–
Ref. [16]	250	~3.5	–
Ref. [17]	61	–	326

To add additional context to our investigations, we sought polarization data on comparable all-vanadium RFBs. At this time, few such studies are publicly available. The three battery configurations we report had overpotentials at 10 mA/cm^2 that are similar to previously reported batteries [15–17], and exhibit comparable cycling characteristics. The ohmic resistances reported by other investigators are very close to the values we measured for the SB, but are nearly an order of magnitude greater than the FCB values. Table 2 summarizes the key data extracted from our polarization studies of the SB, FCB-F, FCB-P and includes applicable data from three other studies. Based on these data, we conclude that lowering activation overpotentials while maintaining a low ASR is a route to improving the performance of RFBs. Though this may seem a self-evident determination, we opine that it merely appears so due to the clarity that polarization curve analysis brings to the table.

We also point out that the present work was carried out with two-electrode cells, as were virtually all contributions discussed in the literature. Under these conditions, it is difficult to directly infer much concerning the relative performance of the two electrodes. What data are available in the literature concerning electrode kinetics and diffusivity for the various species suggest that the two electrodes will behave similarly. Yamamura et al. [18] show

slightly better kinetics for the negative electrode but all results discussed there appear to be highly dependent on the exact carbon material used. Furthermore, reported diffusion coefficients are generally similar. Different data taken from the literature indicates that one or the other D for different oxidation states is somewhat different from the others, but not systematically so. Thus, short of developing and inserting a reference electrode and actually measuring the difference or more thorough experimentation to reveal physical parameters, it is difficult to speculate on the relative performance of the two electrodes. These significant gaps in the literature will be addressed in subsequent contributions.

3.3 Recommendations

The work presented here has resulted in the formulation of some 'best practices' that can be used as guidelines for investigators beginning studies of RFBs.

(1) Galvanostatic control is preferable to potentiostatic control for acquisition of polarization curves, resulting in a generally more stable response from the device.
(2) HFR measurements at 15–30 kHz were found to most accurately approximate the DC resistance of our RFBs. This value is somewhat higher than the value of ~1–5 kHz used for the same measurement in PEM fuel cells [14].
(3) Accurate recording of polarization curves requires electrolyte reservoirs containing sufficient volume that a polarization curve will not exhaust the stock of charged vanadium species. Figure 6 shows potentiostatic polarization curves that exhibit a decreasing current density with a lowering of cell potential at the higher limiting currents; this is attributed to exhaustion of the electrolyte.
(4) Polarization curve analysis does not allow the determination of overpotentials at the individual electrodes without the inclusion of a reference electrode. Thus, we cannot ascertain whether cell overpotential is located primarily in the negative electrode, positive electrode, or is distributed between the two. For this reason, reference electrodes are essential for more detailed studies of polarization in RFBs.

4 Conclusion

In this work, polarization curves were utilized to analyze the distribution of performance losses for two different all-vanadium RFB architectures. We considered a SB characterized by thick carbon felt electrodes and a flow-through design and a FCB based on modified DMFC hardware with thin electrodes and serpentine flow fields. Kinetic polarization was nearly absent in the SB, but significant for all conditions explored in the FCB, probably due to the much greater electrode surface area in the SB. In contrast, the iR_{dc} correction was dominant in the SB, but did not significantly affect the polarization curves for the FCB. This was likely due to significant contact resistance losses in the SB while the FCB exhibited more 'pseudo-iR' losses, i.e. limitations in ionic transport through the electrode layers, that were not addressed via iR correction. By identifying different origins of voltage loss in these ostensibly similar devices, we demonstrate the central importance of polarization analysis to the study of RFB systems.

Acknowledgments We gratefully acknowledge the Governor's Chair Fund from the State of Tennessee for support of this research. TZ also acknowledges the support of the Materials Science and Technology Division of the Physical Sciences Directorate at Oak Ridge National Lab for support of this work through coverage of his time. DA and ZT acknowledge SEERC and the Dept. of Chemical and Biomolecular Engineering for their partial support of this work.

References

1. Rychick M, Skyllas-Kazacos M (1988) J Power Sources 22:59–67
2. Skyllas-Kazacos M, Kasherman D, Hong DR, Kazacos M (1991) J Power Sources 35:399–404
3. Dell R (2001) J Power Sources 100:2–17
4. Joerissen L, Garche J, Fabjan C, Tomazic G (2004) J Power Sources 127:98–104
5. Ponce de Leon C, Frias-Ferrer A, Gonzalez-Garcia J, Szanto D, Walsh FC (2006) J Power Sources 160:716–732
6. Fabjan C, Garche J, Harrer B, Jorissen L, Kolbeck C, Philippi F, Tomazic G, Wagner F (2001) Electrochim Acta 47:825–831
7. Sun B, Skyllas-Kazacos M (1992) Electrochim Acta 37: 1253–1260
8. Fang B, Wei Y, Arai T, Iwasa S, Kumagai M (2003) J Appl Electrochem 33:197–203
9. Sun B, Skyllas-Kazacos M (1992) Electrochim Acta 37: 2459–2465
10. Arico V, Creti AS, Antonucci P, Antonucci PL (1998) Electrochem Solid State Lett 1:66–68
11. Yoon KJ, Huang W, Ye G, Gopalan S, Pal UB, Seccombe DA (2007) J Electrochem Soc 154:B389
12. Mench M (2008) Fuel cell engines. Wiley, Hoboken
13. Tang Z, Aaron D, Keith R, Papandrew A, Zawodzinski T Jr (2011) Proceedings of the 220th Electrochemical Society meeting (Submitted)
14. Cooper KR, Smith M (2006) J Power Sources 160:1088–1095
15. Kazacos M, Skyllas-Kazacos M (1989) J Electrochem Soc 136:2759–2760
16. Chen D, Wang S, Xiao M, Meng Y (2010) J Power Sources 195:2089–2095
17. Kjeang E, Michel R, Harrington D, Djilali N, Sinton D (2008) J Am Chem Soc 130:4000–4006
18. Yamamura T, Watanabe N, Yano T, Shiokawa Y (2005) J Electrochem Soc 152:A830–A836